Water and Environment Journal, Volume 32, Issue 4, 2018, pp. 519-526
DOI:10.1111/wej.12349

Fluorescence enabled direct visual observation for diagnosis of ultrafiltration membrane fouling by bidisperse sub-micron particle suspensions

O. Autin[a], H. Sakar[b], E.J. McAdam[a,*]
[a]Cranfield Water Science Institute, Vincent Building, Cranfield University, Bedfordshire, MK43 0AL, UK
[b]Environmental Engineering Department, Gebze Technical University, Gebze, 41400, Turkey
*Corresponding author e-mail: e.mcadam@cranfield.ac.uk

Abstract

Whilst direct observation methodologies can describe back-transport of supra-micron particles, present technologies are unable to discriminate sub-micron particles, which are primarily responsible for membrane fouling. In this study we therefore introduce a fluorescence enabled direct visual observation (RLF-DVO) methodology to permit visual characterisation of sub-micron particle transport during cross-flow filtration. Particle discrimination was achievable for particle diameters exceeding 0.25 μm; however, this was dependent upon particle concentration and the cross-flow velocity employed. Nevertheless, this is considerably below the detection limit of current techniques (around 3 μm). During filtration of a binary dispersion comprised of sub-micron particles, deposition was observed before a change in transmembrane pressure was detected, which underpins the important role of direct observation for fouling diagnosis. Based on observations made during this study, recommendations are proposed that will further improve resolution. Importantly, this study demonstrates RLF-DVO can provide real-time description of sub-micron particle transport during cross-flow filtration.

Keywords: *direct observation, fluorescence, sub-micron, binary*

1. Introduction

Membrane bioreactors (MBRs) are an advanced wastewater treatment technology that enables process intensification and as the ultrafiltration membrane can achieve excellent separation, MBRs are capable of meeting particularly challenging discharge standards (Judd, 2011). Process intensification is fostered through using the membrane for enhanced particulate rejection, which allows solids retention time to be decoupled from hydraulic retention time. However, this promotes particle polarisation at the membrane wall which constrains hydraulic productivity (Jiang et al., 2007). Consequently, gas or liquid pumping is used to introduce shear at the membrane wall, to promote particle back-transport into the bulk, as a means to sustain productivity. This membrane 'fouling' phenomenon has been the focus of extensive research as the energy penalty incurred for introducing shear, coupled with the need to specify excess membrane area to compensate for the reduction in hydraulic productivity, imposes added cost that constitutes a significant barrier to the wider deployment of MBRs (Judd, 2011).

The particle matrix is heterogeneous both in size distribution and origin but broadly contains soluble microbial products (SMP), which are around 0.1 to 1 μm in size, single cell bacteria (0.1 to 5 μm in size), and flocs which comprise of cells and cell fragments embedded in a polymeric network of extracellular polymeric substances (EPS), which are around 5 to 100 μm in size. Several studies have demonstrated that the colloidal (approximate classification, 1.5 to 0.45 μm) and soluble (often classified as <0.45 μm) fractions primarily contribute to fouling (Bouhabila et al., 2001; Grelier et al., 2005; Li et al., 2005b; Itonaga, et al., 2004; Bae and Tak., 2005). The principal constituents of these particle sub-groups are high molecular weight protein and polysaccharide compounds that are commonly below 1μm in size (Figure 1).

Whilst their contribution to membrane fouling is well recognised, the explicit mechanisms which govern membrane fouling by this discrete sub-micron particle group are less well understood [3-5]. This can be accounted for by the complex particle-particle and particle-membrane interactions that occur within the polarised region adjacent to the membrane surface (Neemann et al., 2014).

Furthermore, the combination of drag and convective forces imposed on the particle system when under filtration, introduce complex hydrodynamic behaviour that is known to promote heterogeneous fouling layer morphologies (Neemann et al., 2013, Martin et al., 2014). Specifically, as these compounds are generally colloidal in nature, their transport is primarily controlled by Brownian motion and as such the shear forces applied to the membrane surface are insufficient to provide back-transport toward the bulk which results in preferential colloidal deposition at the membrane (McAdam et al., 2011).

Direct Observation (DO) describes a group of methodologies that enable non-invasive characterisation of particles contained within the 'critical' polarised region which forms adjacent to the membrane during real-time filtration (Autin et al., 2016). Zhang et al. (2006) used Direct Observation Through Membrane (DOTM) to study particle-particle interaction within bidisperse suspensions, comprised of particles ranging 3 to 10 µm in diameter. The authors demonstrated that the critical flux of smaller particles increased, ostensibly due to the larger particles augmenting shear induced diffusivity of the smaller particles. Marselina et al. (2009) developed Direct Visual Observation (DVO) which oriented the camera tangentially to a hollow fibre membrane. As such, the DVO method permitted new information to be determined, as the velocity profiles of particles near the membrane surface could be quantified during filtration, enabling classification of both stagnant and fluidised regions within the subsequently formed deposit. Whilst both studies provide significant insight into particle-particle interaction and particle back-transport, the techniques rely on visible light for detection, which limits quantitation to particles around 3 µm or greater in diameter (Le-Clech et al., 2007). Consequently, the sub-micron particle fraction, which is recognised to form more tenacious foulant layers, has not been well studied. This is important as the enhancement in mass transport provided within micron sized binary dispersions, previously reported using DOTM (Li et al., 2000; Zhang et al., 2006), is in contradiction to previous research which evidenced a reduction in critical flux in a binary dispersion comprised sub-micron particles (Madaeni et al., 2006).

Within other disciplines, reflected light fluorescence (RLF) has been used to enhance particle resolution through employing light of a prescribed wavelength to excite an auto-fluorescing fluorochrome. For example, in aquatic microbiology, RLF has been used to enable counting of viruses below 1 μm in size (Noble and Fuhrman, 1998). In this study, we therefore propose to integrate reflected light fluorescence into DVO methodology to enable, for the first time, the direct measurement of sub-micron particles within binary dispersions, undergoing filtration. Specifically, we will: (i) demonstrate RLF-DVO for the characterisation of sub-micron particles; (ii) use RLF-DVO to quantify particle back-transport of sub-micron and super-micron particles; (iii) compare classical pressure based and deposition based methods for the determination of critical flux in binary dispersions comprised of sub-micron particles.

2. Materials and methods

2.1 Experimental Set-up

The microscope was equipped with reflected light fluorescence (RLF) detection to provide emission at specific wavelengths (DM5500B, Leica Microsystems, Milton Keynes, UK). A digital high speed camera (DFC365 FX, Leica Microsystems, Milton Keynes, UK) was mounted on the microscope for image collection and analysed using Leica Application Suite software and VideoStudio software for particle tracking (Ulead, Malavida). A crossflow filtration cell was mounted onto the microscope stage; a viewing window was routed into the top of the cell to enable imaging. A PVDF hollow fibre membrane with fitted within the channel and operated in an 'out-to-in' filtration mode. The ultrafiltration (0.04 μm) hollow fibre membrane had an outside diameter of 0.0019 m, and an active surface area of 0.00125 m^2 (Zeeweed, GE Power and Water, Ontario, USA). The 'fluid-gap' between the outer fibre wall and the viewing window was around 2.5 mm. The filtration cell was fitted with pressure transducers with a reported sensitivity of <0.25% of range, on the retentate (0–1 barg) and permeate (+0.5 to -0.5 barg) channel to measure transmembrane pressure (TMP). Critical flux (J_c) was experimentally determined by assuming TMP of the suspension remain equal to the TMP of

clean water at the corresponding flux provided there is no deposition (Field et al., 1995). Particle polarisation will occur at the membrane wall once the convective force (applied by the permeate pump) exceeds the force applied by diffusive back-transport. Back-transport is described by Brownian diffusion (Eq. 1), shear induced diffusion (Eq. 2), which refers to particle motion induced by particle-particle interaction in a shear flow [Rusconi and Stone, 2008, Tardieu et al., 1998), and inertial lift (Eq. 3), which describes convective interaction between particles and the surrounding undisturbed flow field (Li et al., 2000; Tardieu et al., 1998):

$$J = 1.31\gamma^{1/3} a^{-2/3} D_{BO}^{2/3} \left(\frac{\phi_W}{\phi_B} \right)^{1/3} L^{-1/3} \quad (1)$$

$$J = 0.078\ \gamma a^{4/3} L^{-1/3} \ln\left(\frac{\phi_W}{\phi_B} \right) \quad (2)$$

$$J = 0.036 \left(\frac{\rho a^3 \gamma^2}{\eta} \right) \quad (3)$$

Numerous models have been derived to predict packing efficiency in binary dispersions. In the Cavern model, there is an assumption that small particles fill the cavities remaining in a packed bed constructed by large particles:

$$\varepsilon_{f,av} = \frac{\phi_L - 1 + \varepsilon_L}{\phi_L} \quad (4)$$

where Ø is the volume fraction of particles, and the subscript L represents large particles. An alternate proposition is that some small particles are replaced by several large particles in a packed bed constructed mostly of small particles. The packing density can also be estimated by material balance (Hwang and Lin, 2016; German, 1989):

$$\varepsilon_{f,av} = 1 - \frac{1 - \varepsilon_s}{1 - \varepsilon_s \phi_L} \quad (5)$$

where the subscript s represents small particles. As both cake porosity and particle volume fraction are smaller than one, the cakes formed by dual-size particles have smaller porosity than that of a

uniform-sized mono-dispersion. The lowest porosity can be given by the intersection point of the curves plotted using (4) and (5):

$$\varepsilon_{av} = \varepsilon_s \varepsilon_L \quad (6)$$

The final average volume fraction, $\emptyset_{av}$ can then be estimated by $1-\varepsilon_{av}$ and can be applied to estimate m_f in a binary particle suspension.

2.2 Chemicals used

Fluorochrome enabled latex microspheres were used as candidate particles (from 0.25 to 10 µm), which are hard dyed to limit bleeding (Firefli™, Thermo Fisher Scientific, US). Green microspheres were used for mono-dispersion testing which have an excitation/emission spectrum of 468/508 nm. Red 3µm microspheres were used for binary testing which exhibit excitation/ emission at 542/612 nm. Model solutions were prepared from microsphere concentrates containing 1% solids and diluted to the desired concentration in ultrapure water (Purelab Option – S7/15, 18.2 MΩ cm^{-1} and TOC < 3 ppb) to which 20 mM sodium chloride) and 1 mM sodium hydrogen carbonate were added to increase ionic strength and buffering capacity of the water (Fisher Scientific, Loughborough, UK). Unless otherwise stated, experiments were run for 3h using a flux (J) of 100 l m^{-2} h^{-1}, and an initial particle concentration of 25 mg l^{-1} at a cross flow velocity (V_L) of 11 mm s^{-1}.

3. Results

3.1 Verification of particle identification and fouling characterisation in mono-dispersions

Using RLF-DVO, particle visualisation was initially undertaken to define the operating conditions at which discrete particles of fixed diameters could be determined (Table 1). Individual particle determination of 0.1 µm particles, could only be determined when crossflow velocity approached stagnation (0 m s^{-1}). For particles diameters between 0.25 and 1 µm, particle discretisation was similarly dependent upon cross flow velocity but also particle concentration. Discrimination of 3 µm particles was independent of concentration or crossflow velocity. For subsequent experiments, V_L

was fixed to 0.011 m s^{-1} which ensured good resolution for particle diameters exceeding 0.5 µm across a range on solution concentrations and is analogous to that successfully applied in earlier experiments (Autin and McAdam, 2015; Autin et al., 2016).

Fouling assessment was undertaken for mono-dispersions with particle diameters 0.25, 0.5, 1, 3, 5, 10 µm (Figure 3). For the smallest particle sizes, starting at a particle diameter of 0.25 µm, d*P*/d*t* was observed to increase as particle diameter increased. Conversely, for the large particle sizes, d*P*/d*t* was observed to increase as particle size reduced. The highest fouling rate was recorded for the mono-dispersion comprised of 1 µm diameter particles. Fouling data was compared to back-transport velocity modelling which evidenced a minimum backtransport velocity at 1 µm, which is coincident with measurement of the highest d*P*/d*t*. Particle back-transport velocity for 0.5 and 3 µm mono-dispersions were measured between 10 and 150 µm from the membrane surface (Figure 4). Higher particle velocities were determined further from the membrane surface. Back-transport velocities appeared similar for both 0.5 and 3 µm mono-dispersions, and were considerably below the crossflow velocity of 11000 µm s^{-1}.

3.2 Fouling characterisation in binary dispersions

Critical flux (J_c) assessment was undertaken on mono-dispersions and bi-dispersions, using pressure as a surrogate determination of fouling (Figure 5). For the 3 µm mono-dispersion, increasing bulk concentration reduced J_c considerably. Lower J_c was attained with the 0.25, 0.5 and 1 µm mono-dispersions. Critical flux measured within the binary dispersion, was similar to that of the 0.25 µm mono-dispersion. Assessment of the binary dispersion comprising 0.5 and 3 µm diameter particles, evidenced a reduction in J_c. In contrast, for the binary dispersion comprised of 1 and 3 µm diameter particles, J_c increased and was increasingly evident at higher particle concentrations. Particle deposition of the 0.5 and 3 µm bi-dispersion was evaluated during critical flux analysis through quantitation of cake height (H_c) (Figure 6). Deposition was evidenced from the outset of filtration.

4. Discussion

Within this study, the application of fluorescence enabled direct visual observation has been evidenced to permit the quantification of particle back transport for dispersions comprised of sub-micron particles. There have previously been very few studies of binary dispersions comprised of sub-micron particles, due to method detection limits of existing methodologies (Le-Clech et al., 2007). Particle back-transport velocities of 0.5 and 3 µm particles were within the range reported by Marselina et al. (2009) for bentonite particles exposed to a CFV of 15 mm s^{-1}. The authors similarly noted particle velocity to increase further from the membrane (below the nominal CFV), which was accounted for by the heterogeneous distribution of fluid velocity within the channel. In this study, particle velocity for 0.5 and 3 µm particles was similar. Caldwell (2000) described an analogous separation problem in which small and large particles 'co-eluted' during field-flow fractionation (FFF), where a flatsheet crossflow filtration cell is used to replace packed columns for the chromatographic separation of particles. Sub-micron particles are driven by the field toward the membrane, increasing the particle wall concentration, which increases the opposing diffusive flux proportionately until an equilibrium is reached with field-driven transport toward the wall (Giddings, 2000). The result is a particle cloud which comprises of an equilibrium distribution whose concentration declines exponentially with distance from the membrane wall (Giddings, 2000). Consequently, whilst 0.5 and 3 µm particle velocities are quantitatively similar within this hydrodynamic range, the different primary back-transport mechanisms impose contrasting particle distributions within the flow. This was visually illustrated when operated at analogous particle volume fractions (Figure 7). For dilute suspensions of large particles exposed to high shear, preferential segregation from the membrane surface is promoted (Krompcamp et al., 2006). In this study, wall shear rate was constrained to ensure visibility of individual particles. It is proposed that limited accumulation of 3 µm particles at the wall could have also been promoted by the wide 'fluid gap' adopted (2.5mm) which reduced the probability for particles migrating to the wall from the faster stream-lines in the centre of the channel. In FFF, a 250 µm channel height is used to ensure

particle migration is controlled through both convective and diffusive forces (Giddings, 2000). The recommended breadth to thickness aspect ratio (b/w) for FFF is ~100 (Barman et al., 1993). For comparison, the present b/w is around 2. Decreasing channel depth will increase b/w to 24, which will extend the parabolic flow profile in the radial direction, thereby improving particle distribution. The consequential impact will be the improved control over particle migration, enabling more refined governance of particle deposition, providing improved and significant insight into particle-particle interaction and particle deposition of the sub-micron particle fraction, which is the critical particle fraction to influence fouling in cross-flow filtration.

Analysis of mono-dispersions indicated 1 µm diameter particles presented the highest fouling rate. This was coincident with the onset of the minimum back-transport velocity and is analogous to earlier description of ultrafiltration for silica particle suspensions between 0.025 and 20 µm (Fane, 1984). Evaluation of particle deposition during critical flux determination of binary dispersions, demonstrated particle deposition was noted by RLF-DVO in advance of TMP detection (Figure 6). Such discontinuity has been previously observed in the study of super-micron suspensions. The authors ascribed the TMP 'lag time' to low pressure transducer sensitivity, insufficient particle accumulation to impose a detectable increase in pressure, and the low specific resistance provided by the foulant (Zhang et al., 2006). Importantly, this evidences the powerful resolution of this RLF-DVO methodology, compared to conventional methods, in enabling the characterisation of sub-micron particle deposition. Krompcamp et al. (2006) reported that only small particles in super-micron bi-dispersions under cross-flow were deposited at the membrane, as these have lower critical fluxes (Li et al., 1998) and proposed that J_c of the small particles could be provided by:

$$J_c = 0.072\gamma_0 \left(\frac{\emptyset_w a^4}{\emptyset_b L}\right)^{1/3} \quad (7)$$

For the specified shear rate, their model estimates J_c of 0.5, 1.4 and 3.4 L m^{-2} h^{-1} for 0.25, 0.5 and 1 µm particles respectively which provides supportive explanation for early deposition in this study (Figure 6). Higher particle back-transport could have been achieved by increasing shear rate,

particularly for binary dispersions comprised of 1 µm particles. However, RLF-DVO is currently limited to shear rates <50 s^{-1} to ensure measurement of particles as individual entities. The proposed changes to the aspect ratio, specifically reducing the distance between the outer fibre wall and viewing window, will also reduce the overall distance to the microscope objective. Whilst the current set-up dimensions were within the working distance of the lens (11 mm; Autin et al., 2016), this will inevitably improve resolution, enabling individual particle identification at higher velocities and across a broader range of concentration and particle size ranges than presently possible (Table 1), helping to further advance understanding of sub-micron particle interactions in complex dispersions.

The particle deposition visually observed in binary dispersions, indicates that by definition, the critical flux was exceeded near the onset of filtration. Consequently, the TMP data provides indicative information of cake formation in the 'super-critical' state (i.e. post-particle deposition) rather than a definitive force-balance determination (Figure 5). For 0.25 µm particles, J_c was ostensibly similar between the mono-dispersion and bi-dispersion. It is proposed that the preferential deposition of 0.25 µm particles in the bi-dispersion resulted in the formation of a cake with similar characteristics (Krompcamp et al., 2006). Increasing sub-micron particle diameter from 0.25 to 0.5 µm reduced J_c of the bi-dispersion. Madaeni (1998) similarly identified that J_c of a bi-dispersion comprising sub-micron particles was below J_c of the mono-dispersion (50 nm gold-sol, 1 µm latex). The authors used invasive imaging to evidence that large particles within the cake increased packing density and hence deposition resistance; this phenomenon being dependent upon the particle fraction. In the transition from 0.25 to 0.5 µm, sub-micron particle number in the bulk decreased by almost an order of magnitude and the relative proportion of 3 µm particles increased from 0.058% to 0.46%. This particle number fraction is the same order as Madaeni et al. (1998). The estimated porosity for the 0.5 µm mono-dispersion was 0.33, compared to only 0.23 for the bi-dispersion, which is similar to cakes produced from bi-dispersions with particle size ratios of 0.01 to 0.06 (Madaeni et al., 1998). The J_c of 1 and 3 µm bi-dispersion was above the J_c of the mono-dispersion (Figure 5) and is analogous to observations by Zhang et al. (2006) for super-micron binary

dispersions in which SID dominated back-transport (ranging 3 to 10 µm). Whilst the specific mechanisms require elucidation, it is apparent that in the super-critical state (i.e. post-particle deposition), the impact of bigger particles is dependent upon the relative particle number fraction in the cake.

5. Conclusions

Within this study, fluorescence enabled DVO has been evidenced to permit direct measurement of sub-micron particles in the binary dispersion. A limiting particle diameter of 0.1 µm was identified at which individual particles could not be discriminated in cross-flow. For particles exceeding 0.25 µm, resolution was determined to be a function of concentration and crossflow velocity. It is asserted that enhanced control of particle migration can be facilitated through selection of a shallower channel depth. Hydrodynamic conditions were selected to enable evaluation of an example binary dispersion compised of 0.5 and 3 micron particles, in which sub-micron particle back-transport was measured through direct observation for the first time. Through comparison of mono-dispersion and bi-dispersion data, it is suggested that particle deposition at low fluxes is primarily by sub-micron particles due to their lower particle critical flux. Higher shear rates could have improved back-transport but RLF-DVO is currently limited to wall shear rates <50 s^{-1} to ensure single particle discrimination. We suggest the shallow depth channel will increase microscope resolution by reducing overall distance between microscope objective and membrane wall, which will enable higher fluid velocities to be evaluated without influencing image quality. Since RLF-DVO does not rely on natural light for luminescence, we consider that the methodology is equally valid for application to flat-sheet DOTM methods, whose membrane selection has been previously limited to those with a capillary pore structure as they enable light transmission. The methodology enabled determination of the early onset of particle deposition, before pressure measurement determined the critical flux which supports earlier observations of methods capable of determining super-micron bi-dispersions, underpinning the importance of direct observation methodologies for diagnostic

investigation of fouling. Importantly, this study demonstrates fluorescence enabled direct observation can provide new insight into particle-particle and particle-membrane interactions for sub-micron particle transport during cross-flow filtration, which has been seldom described due to the limitations of previous techniques.

Acknowledgments

The authors thank the Engineering and Physical Sciences Research Council for financial support (EPSRC, EP/K010360/1) and The Scientific and Technological Research Council of Turkey (TUBITAK), who provided a scholarship for Sakar. Enquiries for access to the data referred to in this article should be directed to: researchdata@ cranfield.ac.uk.

References

B.N. Barman, M.N. Myers, J.C. Giddings, Rapid particle size analysis of ground minerals by flow/hyperlayer field-flow fractionation. Powder Technol. 59 (1989) 53-63.

E.H. Bouhabila, R. Ben Aim, H. Buisson, Fouling characterisation in membrane bioreactors, Sep. Purif. Technol. 22-23 (2001) 123-132.

I. Martin-Garcia, V. Monsalvo, M. Pidou, P. Le-Clech, S.J. Judd, E.J. McAdam, B. Jefferson, Impact of membrane configuration on fouling in anaerobic membrane bioreactors, J. Membr. Sci. 382 (2011) 41-49.

P. Grelier, S. Rosenberger, A. Tazi-Pain, Influence of sludge retention time on membrane bioreactor hydraulic performance, In: Proceedings of international congress on membranes and membrane processes (ICOM), Seoul, June 7-10.

T. Itonaga, K. Kimura, Y. Watanabe, Influence of suspension viscosity and colloidal particles on permeability of membrane used in membrane bioreactor (MBR), Water Sci. Technol. 50 (2004) 301-309.

T. Jiang, M.D. Kennedy, C. Yoo, I. Nopens, W. van der Meer, H. Futselaar, J.C. Schippers, P.A. Vanrolleghem, Controlling submicron particle deposition in a side-stream membrane bioreactor: A theoretical hydrodynamic modelling approach incorporating energy consumption, J. Membr. Sci. 297 (2007) 141-151.

S. Judd, C. Judd, The MBR Book: Principles and applications of membrane bioreactors for water and wastewater treatment, 2011, 2nd Edition, Butterworth-Heinemann, Oxford, UK.

T.-H. Bae, T.M. Tak, Interpretation of fouling characteristics of ultrafiltration membranes during the filtration of membrane bioreactor mixed liquor, J. Membr. Sci. 264 (2005) 151-160.

E.J. McAdam, E. Cartmell, S.J. Judd, Comparison of dead-end and continuous filtration conditions in a denitrification membrane bioreactor, J. Membr. Sci. 369 (2011) 167-173.

F. Neemann, S. Rosenberger, B. Jefferson, E.J. McAdam, Non-covalent protein–polysaccharide interactions and their influence on membrane fouling, J. Membr. Sci. 446 (2013) 310-317.

K.J. Martin, D. Bolster, N. Derlon, E. Morgenroth, R. Nerenberg, Effect of fouling layer spatial distribution on permeate flux: A theoretical and experimental study, J. Membr. Sci. 471 (2014) 130-137.

Y.P. Zhang, A.G. Fane, A.W.K Law, Critical flux and particle deposition of bi-disperse suspensions during crossflow filtration, J. Membr. Sci. 282 (2006) 189-197.

O. Autin, F. Hai, S. Judd, E. McAdam, Investigating the significance of coagulation kinetics on maintaining membrane permeability in an MBR following reactive coagulant dosing, J. Membr. Sci. 516 (2016) 64-73.

Y. Marselina, Lifia, P. Le-Clech, R.M. Steutz, V. Chen, Characterisation of membrane fouling deposition and removal by direct observation technique, J. Membr. Sci. 341 (2009) 163-171.

H. Li, A.G. Fane, H.G.L. Coster, S. Vigneswaran, Assessment of depolarisation models of crossflow microfiltration by direct observation through membrane, J. Membr. Sci. 172 (2000) 135-147.

P. Le-Clech, Y. Marselina, Y. Ye, R.M. Stuetz, V. Chen, Visualisation of polysaccharide fouling on microporous membrane using different characterisation techniques, J. Membr. Sci. 290 (2007) 36-45.

R. Noble, J. Fuhrman (1998). Use of SYBR Green I for rapid epifluorescence counts of marine viruses and bacteria Aquatic Microbial Ecology, 14, 113-118.

O. Autin, E.J. McAdam, Method and apparatus for monitoring particles in a liquid, GB Patent Application No. 1516481.7 (2015)

R. Rusconi, H.A. Stone, Shear-induced diffusion of platelike particles in microchannels, Phys. Rev. Lett. 101 (2008).

E. Tardieu, A. Grasmick, V. Geaugey, J. Manem, Hydrodynamic control of bioparticle deposition in a MBR applied to wastewater treatment, J. Memb. Sci. 147 (1998) 1-12.

K.-J. Hwang, I.-L. Lin, Effects of mixing ratio of binary fine particles on the packing density and filtration characteristics, KONA Powder Part. J. 33 (2016) 296-303.

J. Calvin Giddings, The Field-Flow Fractionation Family: Underlying principles. *In:* Field-Flow Fractionation Handbook. Eds. M. Schimpf, K. Caldwell. J. Calvin Giddings (2000) Wiley & Sons, NY, US

K.D. Caldwell, Steric Field-Flow Fractionation and the Steric Transition. *In:* Field-Flow Fractionation Handbook. Eds. M. Schimpf, K. Caldwell. J. Calvin Giddings (2000) Wiley & Sons, NY, US

R.W. Field, D.X. Wu, J.A. Howell, B.B. Gupta, Critical flux concept for microfiltration fouling, J. Membr. Sci. 100 (1995) 259-272.

A.G. Fane, Ultrafiltration of suspensions, J. Membr. Sci. 20 (1984) 249-259.

S.S. Madaeni, A.G. Fane, Microfiltration of very dilute colloidal mixtures, J. Membr. Sci. 113 (1996) 301-312.

S.S. Madaeni, Ultrafiltration of very dilute colloidal mixtures, Colloids Surf. A 131 (1998) 109-118.

S.S. Madaeni, The effect of operating conditions on critical flux in membrane filtration of latexes, Trans. IChemE 75 (1997) 266-269.

J. Krompcamp, M. van Domselaar, K. Schroen, R. van der Sman, R. boom, Shear-induced diffusion model for microfiltration of polydisperse suspensions, J. Membr. Sci. 146 (2002) 63-68.

H. Li, A.G. Fane, H.G.L. Coster, S. Vigneswaran, A.G. Fane, Direct observation of particle deposition on the membrane surface during crossflow microfiltration. J. Membr. Sci. 149 (1998) 83-97.

J. Krompcamp, F. Faber, K. Schroen, R. Boom, Effects of particle size segregation on crossflow microfiltration performance: control mechanism for concentration polarisation and particle fractionation, J. Membr. Sci. 268 (2006) 189-197.

S.T.V. Sim, A.H. Taheri, T.H. Chong, W.B. Krantz, A.G. Fane, Colloidal metastability and membrane fouling – Effects of crossflow velocity, flux, salinity and colloid concentration, J. Membr. Sci. 469 (2014) 174-187.

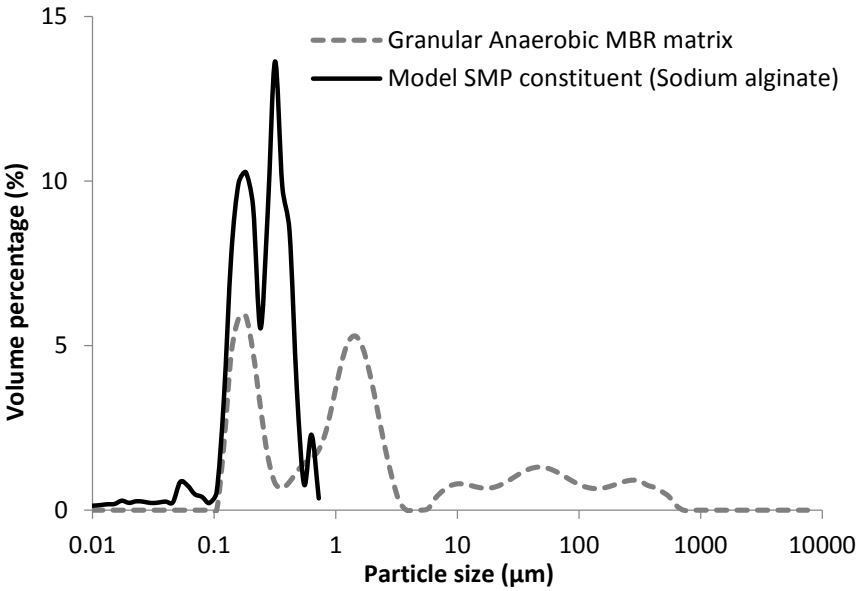

Figure 1. Particle size distribution of an anaerobic MBR used to evidence bimodal distribution, with a peak in the sub-micron range. This is compared the model polysaccharide Sodium Alginate, often used as a surrogate of SMP, whose particle size is within the sub-micron range.

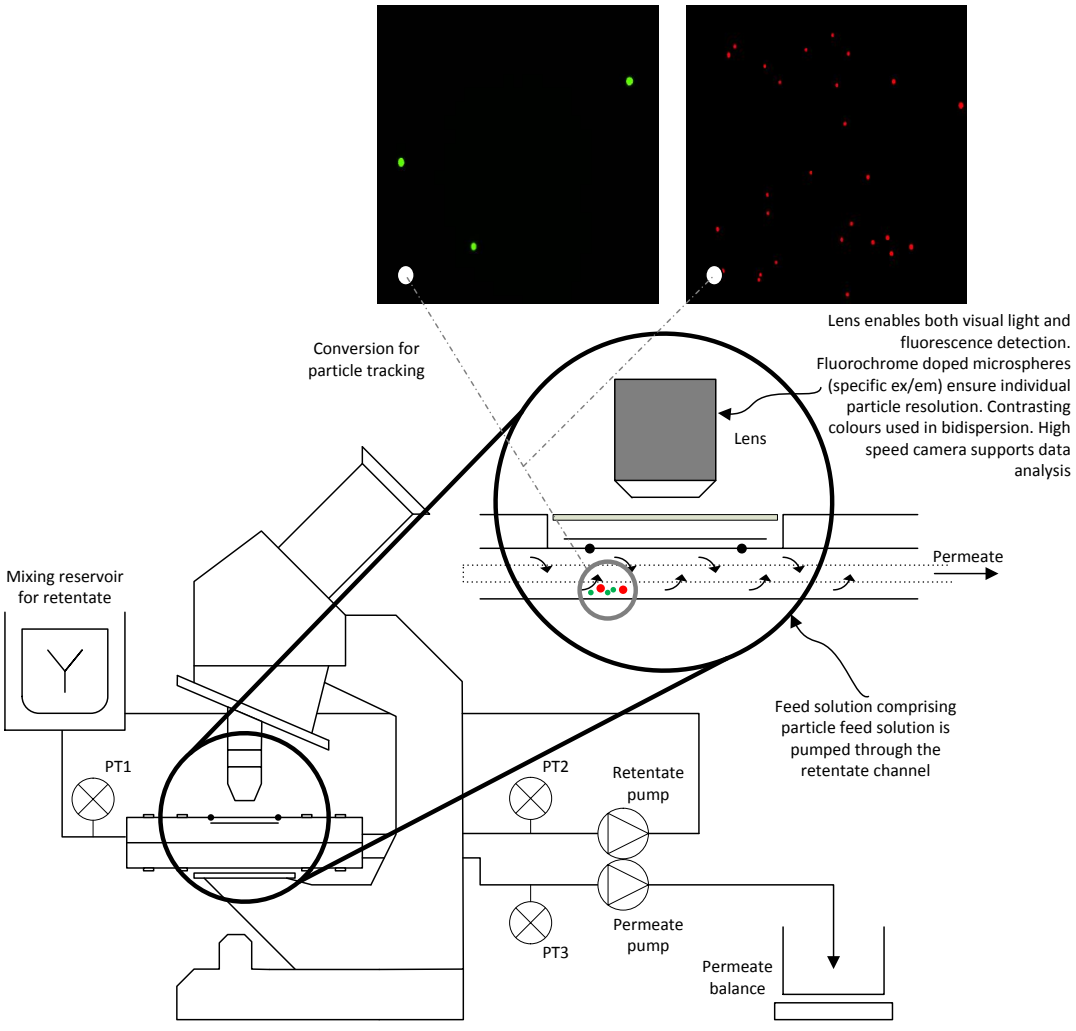

Figure 2. Experimental set-up.

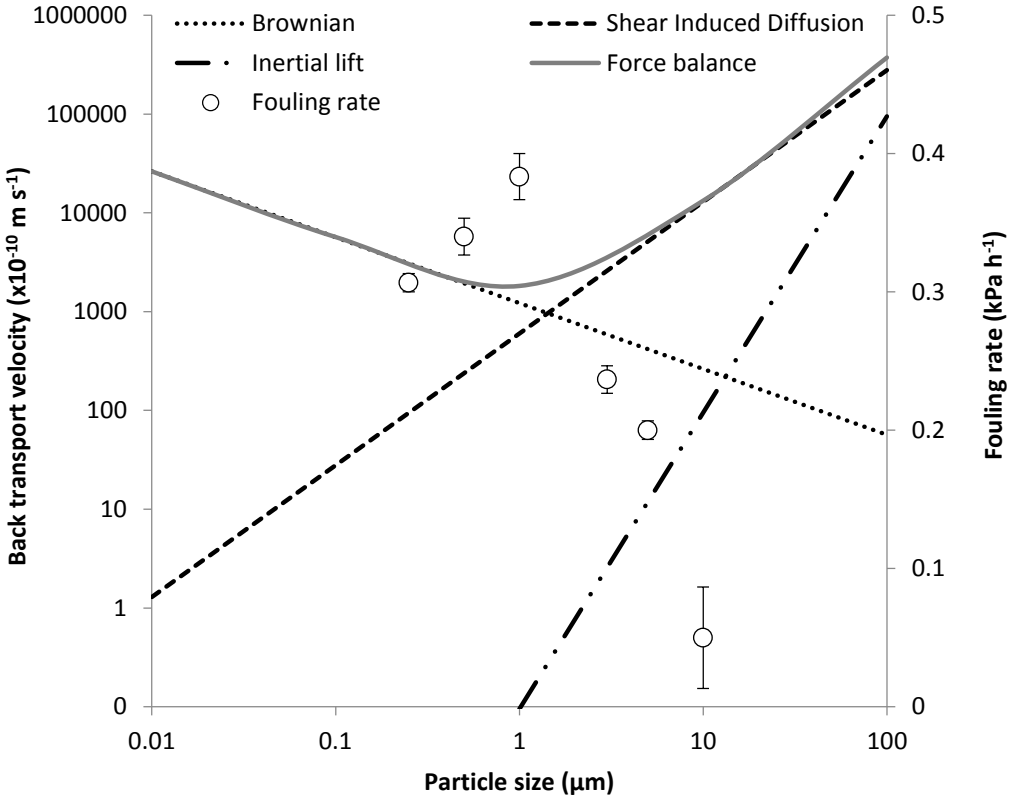

Figure 3. Fouling rate determined for particle mono-dispersions and compared to modelled back-transport velocities (0.25 to 10 µm). C_b 0.01 kg m^{-3}; V_L 0.011 m s^{-1}.

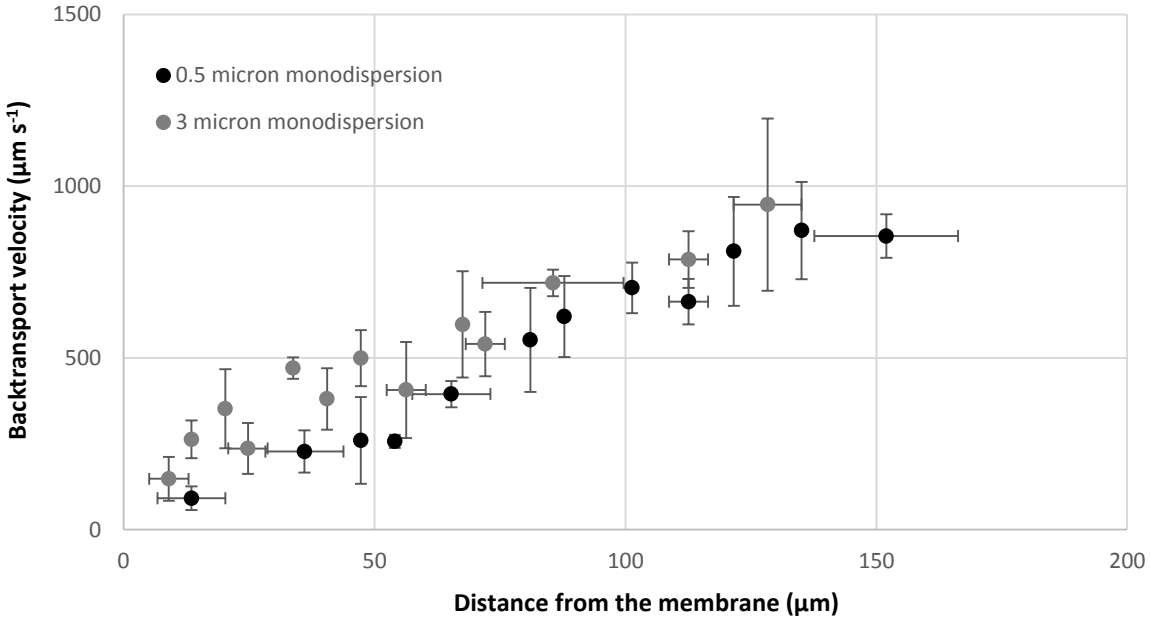

Figure 4. Measured particle back-transport velocities (µm s^{-1}) for particle mono-dispersions in the polarised region adjacent to the membrane. C_b 0.01 kg m^{-3}; V_L 0.011 m s^{-1}.

(a)

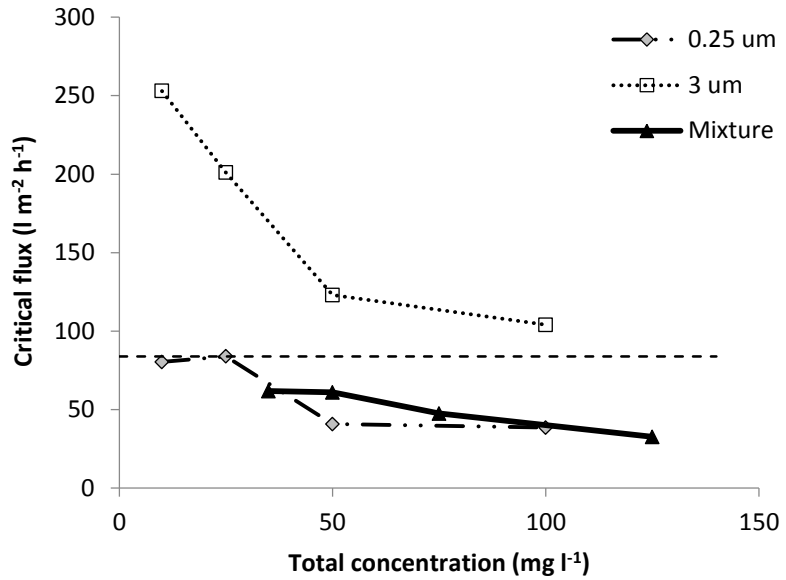

(b)

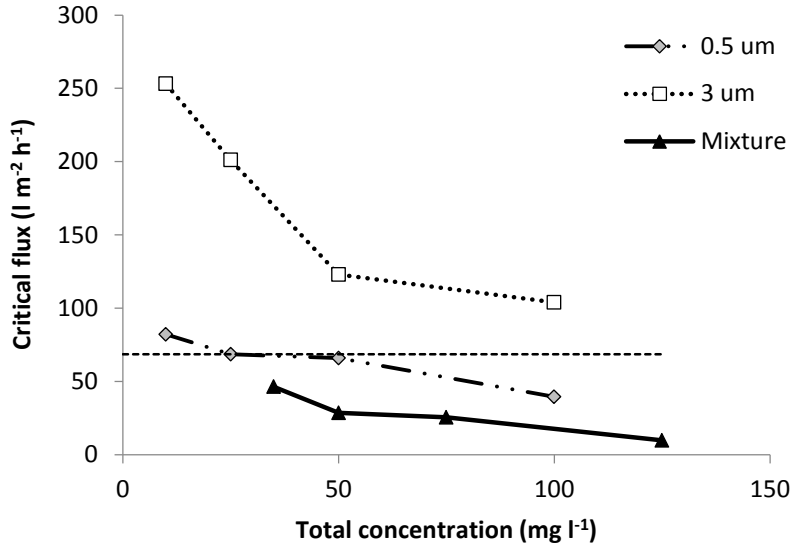

(c)

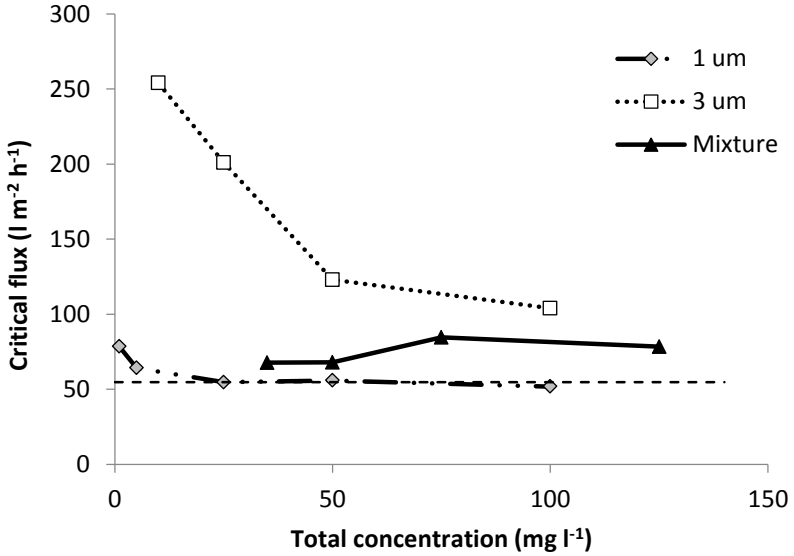

Figure 5. Critical flux (J_c) determination for mono-dispersions and binary dispersions using the flux-step method. C_b 0.01 kg m^{-3}; V_L 0.011 m s^{-1}.

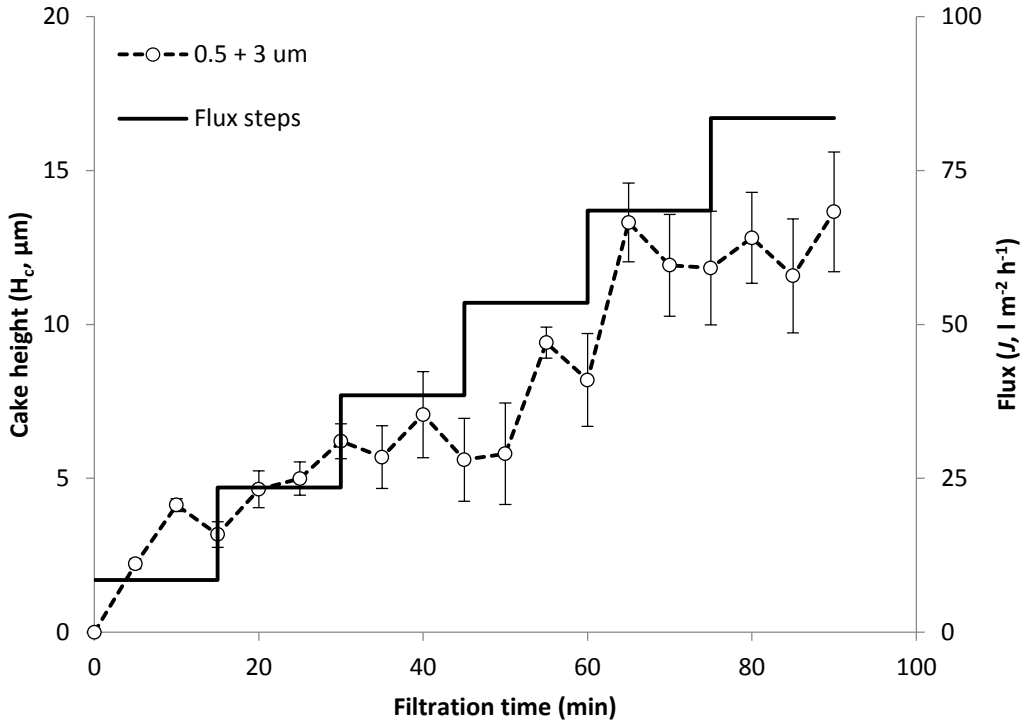

Figure 6. Particle deposition determined for binary dispersions of 0.5+3 µm and 1+3 µm, when using the flux-step method. C_b 0.01 kg m^{-3}; V_L 0.011 m s^{-1}.

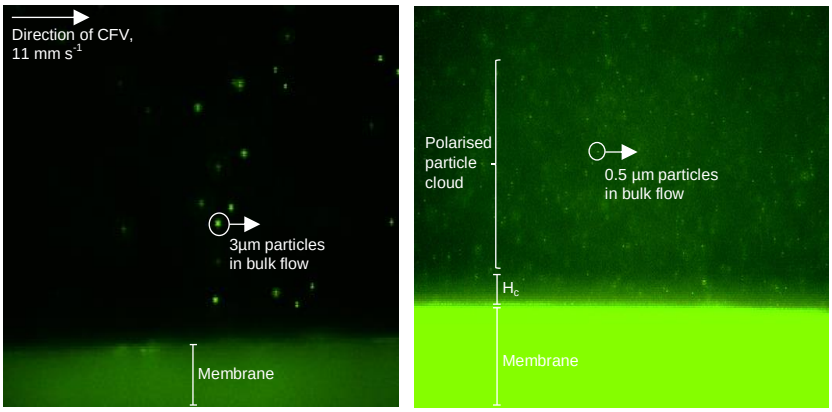

(a) 3µm (b) 0.5µm

Figure 7. Raw images captured in real-time during ultrafiltration of mono-dispersions undergoing ultrafiltration: C_b, 10 mg l^{-1}; CFV, 0.011 m s^{-1}. Magnification: 10x (3 µm); 20x (0.5 µm).

Table 1. Individual particle resolution for reflected light fluorescence direct observation methodology (RLF-DVO) when particles are exposed to cross-flow

Cross-flow velocity (m s^{-1})	Particle size under testing (µm)/ Particle concentration (mg l^{-1})																								
	0.1					0.25					0.5					1					3				
	0.1	1	10	25	50	0.1	1	10	25	50	0.1	1	10	25	50	0.1	1	10	25	50	0.1	1	10	25	50
0	✓	✓	✓	✓	✓	✓	✓	✓	✓	✓	✓	✓	✓	✓	✓	✓	✓	✓	✓	✓	✓	✓	✓	✓	✓
0.001	×	×	×	×	×	✓	✓	✓	✓	✓	✓	✓	✓	✓	✓	✓	✓	✓	✓	✓	✓	✓	✓	✓	✓	✓
0.005	×	×	×	×	×	✓	✓	✓	✓	×	✓	✓	✓	✓	×	✓	✓	✓	✓	✓	✓	✓	✓	✓	✓	✓
0.011	×	×	×	×	×	✓	✓	×	×	×	✓	✓	✓	✓	×	✓	✓	✓	✓	✓	✓	✓	✓	✓	✓	✓
0.05	×	×	×	×	×	×	×	×	×	×	✓	✓	✓	×	×	✓	✓	✓	✓	×	✓	✓	✓	✓	✓	✓
0.1	×	×	×	×	×	×	×	×	×	×	×	×	×	×	×	✓	✓	×	×	×	✓	✓	✓	✓	✓	✓